Effect of Dipole Mobility in Secondary Crystals on Piezoelectricity of a Poly(vinylidene fluoride-co-trifluoroethylene) 52/48 mol% Random Copolymer with an Extended-chain Crystal Structure

Zhiwen Zhu¹, Guanchun Rui², Ruipeng Li³, Hezhi He^{1,*}, Lei Zhu^{2,*}

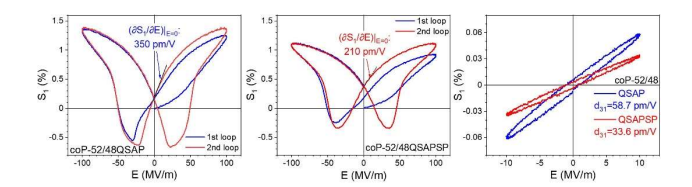
National Engineering Research Center of Novel Equipment for Polymer Processing, Guangdong
 Provincial Key Laboratory of Technique and Equipment for Macromolecular Advanced
 Manufacturing, South China University of Technology, Guangzhou, 510641, P. R. China

 Department of Macromolecular Science and Engineering, Case Western Reserve University,
 Cleveland, Ohio 44106-7202, United States

³ National Synchrotron Light Source II, Brookhaven National Laboratory, Upton, New York 11973, United States

* Corresponding authors. Emails: lxz121@case.edu (L. Zhu) and pmhzhe@scut.edu.cn (H. He)

Table of Content Graphic



Abstract

High performance piezoelectric polymers are promising for a broad range of practical applications, such as sensors, actuators, and energy generators in medical devices, wearable electronics, and soft robotics. Recently, giant piezoelectricity was reported for poly(vinylidene fluoride-co-trifluoroethylene) [P(VDF-TrFE)] copolymers with the composition around 50/50 mol%, which was attributed to the relaxor-like secondary crystals (SCs) in the oriented amorphous fraction (SC_{OAF}). However, it was still unclear how the dipole mobility in the SC_{OAF} affect the piezoelectricity of ferroelectric polymers. In this work, we compared two P(VDF-TrFE) 52/48 mol% samples with an extended-chain crystal structure. The first sample was hot-pressed, quenched, stretched, 130 °C-annealed, and unidirectionally poled at 100 MV/m (denoted as coP-52/48QSAP). After additional uniaxial stretching of coP-52/48QSAP at 6% followed by electric poling, the coP-52/48QSAPSP film was obtained. Intriguingly, coP-52/48QSAPSP exhibited much lower piezoelectric performance than coP-52/48QSAP at room temperature. Based on a broadband dielectric spectroscopy study, it was found that the dipole mobility in coP-52/48QSAPSP significantly decreased as compared to coP-52/48QSAP. It was the lower dipole mobility that decreased the piezoelectric performance for coP-52/48QSAPSP. However, upon heating toward the melting temperature (~58 °C) of the SC_{OAF}, the dipole mobility was regained, and high piezoelectric performance was achieved at 50 °C: the piezoelectric strain constant d_{31} = 62.5 ± 7.2 pm/V and the electromechanical coupling factor $k_{31} = 0.123$. This understanding of the dipole mobility in SC_{OAF} will provide us a guidance to achieving high piezoelectric performance in other ferroelectric polymers such as PVDF homopolymers.

Introduction

Piezoelectricity refers to a linear electromechanical coupling effect between mechanical stress (or mechanical strain) and charge density (or electric field).¹ The former is the direct piezoelectric effect and the latter is the inverse piezoelectric effect. Two main classes of piezoelectric materials are widely studied: inorganic and organic piezoelectrics. Typical examples are lead zirconate titanate (PZT) ceramics and poly(vinylidene fluoride) (PVDF)-based polymers [including its random copolymers with trifluoroethylene, P(VDF-TrFE)], respectively. Compared with the ceramic counterparts, piezoelectric polymers are promising for sensors, actuators, and energy harvesting in medical devices, wearable electronics, and soft robotics,²⁻⁷ owing to its non-toxicity, flexibility, low cost, and biocompatibility. However, their low piezoelectric coefficient [e.g., $-d_{33}$ and $d_{31} = 20$ -30 pC/N for PVDF and P(VDF-TrFE)] and low energy conversion efficiency ($k^2 = 0.01$ -0.1) limit their practical applications.⁸⁻¹¹ This is largely attributed to the lack of fundamental understanding of piezoelectricity of ferroelectric polymers, although the origin of piezoelectricity has been attributed to the macroscopic (or permanent) remanent polarization (P_{r0})-biased electrostriction.^{9, 12, 13}

In the beginning, piezoelectricity in polymers was considered as a result of the dimensional effect, ¹⁴⁻¹⁷ and the compliant amorphous phase should be primarily responsible for it. Later, it was found that the dimensional effect could not account for 100% piezoelectricity in polymers, and ferroelectric crystals must also play an important role. For example, a recent study showed that a morphotropic phase boundary (MPB)-like behavior (often observed for piezoelectric ceramics¹⁸) was proposed for P(VDF-TrFE) with a composition around 50/50 mol%, and that the piezoelectricity was enhanced by the helical-to-zigzag conformation transformation in the crystalline domains of P(VDF-TrFE) near the MPB. ^{11, 19} However, polymer crystals also could

not account for 100% piezoelectricity (especially for d₃₁), and the amorphous phase must participate to facilitate the high d₃₁ of PVDF.²⁰ Recently, in-situ dynamic X-ray diffraction measurements on a spin-coated P(VDF-TrFE) 65/35 mol% sample suggested that an additional contribution from the electromechanical coupling between the crystalline lamellae and the amorphous regions should be the primary contribution to polymer piezoelectricity.²¹ From our recent work on highly poled biaxially oriented PVDF with a pure β phase, ²² this interfacial coupling was actually realized via the highly mobile, liquid crystal-like oriented amorphous fraction (OAF) between the crystalline lamella and the isotropic amorphous fraction (IAF).²³ Furthermore, if relaxor-like (i.e., highly mobile) secondary crystals (SCs) were induced in the OAF layers (i.e., SC_{OAF}) of the P(VDF-TrFE) copolymers with an extended-chain crystal (ECC) structure, piezoelectricity was further enhanced via the P_{r0}-biased electrostriction.²⁴ For example, the quenched (Q), stretched (S), 130 °C-annealed (A), and electrically poled (P) P(VDF-TrFE) 52/48 mol% copolymer film (coP-52/48QSAP) exhibited a high d₃₁ of 57.6±2.4 pm/V at room temperature. Note, SCs have been reported before for PVDF polymers^{25, 26} and are ascribed to the short -(CH₂CF₂)_n- sequences separated by head-to-head and tail-to-tail (HHTT) defects (usually 5-6 mol%) in PVDF chains.²⁷ Meanwhile, the relaxor-like SC_{OAF} in coP-52/48QSAP was induced by high-field electric poling. Without electric poling, few relaxor-like SC_{OAF} could form in the ECC coP-52/48SQAP film.

Although the above understanding of relaxor-like SC_{OAF} to improve piezoelectricity in the P(VDF-TrFE) random copolymers has been achieved, there is still a question: How does the dipole mobility in SC_{OAF} affect the piezoelectric performance? In this work, the coP-52/48QSAP film is further stretched mechanically up to 6%, followed by unidirectional electric poling at 100 MV/m to achieve a sizable P_{r0} . The resultant sample is denoted as coP-52/48QSAPSP. Intriguingly,

the dipole mobility in SC_{OAF} of coP-52/48QSAPSP dramatically decreases. Inverse piezoelectric tests and structural characterization are performed to compare the piezoelectric performance of coP-52/48QSAP and coP-52/48QSAPSP. The goal is to understand how the dipole mobility in SC_{OAF} affect the piezoelectricity of ferroelectric P(VDF-TrFE) random copolymers.

Experimental Section

Materials. The P(VDF-TrFE) 52/48 mol% random copolymer was kindly supplied by Piezotech/Arkema, Lyon, France. The comonomer composition was determined by proton nuclear magnetic resonance (¹H NMR) spectroscopy.²⁴ The molecular weight and molecular weight distribution were determined by size-exclusion chromatography: the number-average molecular weight was 287,000 g/mol and the dispersity was 2.9.²⁴ The polymer powder was used as received without further purification.

Films Fabrication and Processing. Two types of film samples were fabricated in this work. (1) *coP-52/48QSAP*. Using non-sticking aluminum foils, the P(VDF-TrFE) 52/48 mol% random copolymer was hot-pressed at 200 °C under a pressure of 12000 psi for 5 min, followed by quenching into liquid nitrogen. The quenched film was uniaxially stretched to an extension ratio of ca. 500% with a stretching rate of 12 mm/min using a home-built stretching apparatus at room temperature. The stretched film was annealed at 130 °C for 48 h to achieve the ECC structure using an Instec HCS402 hot stage (Instec, Inc., Boulder, CO). The obtained film was denoted as coP-52/48QSA and was unidirectionally polarized under 100 MV/m (i.e., 50 DC + 50 AC at 1 Hz) for 60 cycles at room temperature to achieve a sizable P_{r0}. The obtained film was denoted as the coP-52/48QSAP film. (2) *coP-52/48QSAPSP*. The coP-52/48QSAP film was uniaxially stretched to an additional strain of ca. 6% at a speed of 1 μm/s using a Linkam TST350

tensile stage (Linkam Scientific, Surrey, UK). The stretched films were unidirectionally polarized under 100 MV/m (i.e., 50 DC + 50 AC at 1 Hz) for 20 cycles at room temperature to achieve a sizable P_{r0} . The obtained film was denoted as coP-52/48QSAPSP. The final thicknesses of all films were around 15-30 μ m.

Characterization and Instrumentation. Differential scanning calorimetry (DSC) experiments were performed on a TA Discovery DSC250 (TA Instruments, New Castle, DE). Approximately 2 mg sample was used at a scanning rate of 10 °C/min under a dry nitrogen atmosphere (flow rate = 50 mL/min). Broadband dielectric spectroscopy (BDS) measurements were carried out using a Novocontrol Concept 80 broadband dielectric spectrometer (Novocontrol Technologies, Montabaur, Germany) with temperature control. The applied voltage was 1.0 V_{rms} (i.e., root-mean-square voltage) with frequency from 1 to 10⁷ Hz and temperature from -50 to 100 °C. The heating rate was 2 °C/min for temperature scans. Gold (Au) electrodes with an area of 7.06 mm² were evaporated on both surfaces of samples using a Quorum Q300T D Plus sputter coater (Quorum Technologies, Ltd., Laughton, East Sussex, UK). The Au electrode thickness was ca. 10 nm.

Two-dimensional (2D) small-angle X-ray scattering (SAXS) and wide-angle X-ray diffraction (WAXD) experiments were performed at the 11-BM Complex Material Scattering Beamline of the National Synchrotron Light Source II (NSLS-II), Brookhaven National Laboratory (BNL). The wavelength (λ) of the incident X-ray was 0.0729 nm. The distances between the sample and the WAXD (Pilatus 800 K, Dectris, Gaden-Dattwil, Switzerland) and the SAXS detectors (Pilatus 2M) were 259 and 5070 mm, respectively. These distances were calibrated using silver behenate with the first-order reflection at a scattering vector of $q = (4\pi \sin\theta)/\lambda = 1.076 \text{ nm}^{-1}$ (θ is the half scattering angle). The typical data acquisition time was 10

s. The final images were generated by the stitching method using custom-developed SciAnalysis program.

Simultaneous electric displacement-electric field (D-E) and transverse strain-electric field (S₁-E) loops were measured using a Premiere II ferroelectric tester (Radiant Technologies, Inc., Albuquerque, NM) with a Trek 10/10B-HS high-voltage amplifier (0-10 kV AC, Trek, Inc., Lockport, NY), as described in previous reports. ²⁹⁻³¹ The applied voltage had a bipolar sinusoidal waveform at 1 Hz. The film samples were coated with Au electrodes on both sides with an overlapping area of 8×3 mm². The uncoated margin on both edges was ~0.3 mm to minimize the constraint of actuation. The Au-coated film was immersed in silicone oil to avoid corona discharge in air. The stray capacitance was determined using a biaxially oriented polypropylene film (8 µm, provided by SB Electronics, Inc., Barre, VT) with a dielectric constant of 2.25. The final electric displacement was obtained by subtracting the stray capacitance and AC electronic conduction from the raw data. The transverse strain, S1, of the film samples (initial length of 8 mm) was measured using a home-built fixture connected to a photonic sensor MTI 2100 (MTI Instruments, Inc., Albany, NY), following the literature reports.²⁹⁻³¹ At high temperatures (>40 °C), significant AC electronic conduction was observed in D-E loops for the large electrode area (24 mm²) copolymer films. To solve this issue, separate D-E loop measurements were performed on small electrode area samples (7.06 mm²). A home-built sample fixture was used to connect the Au electrodes on both sides of the film with the interface of the Radiant ferroelectric tester using high-voltage cables. The temperature was controlled using a ChemGlass CG-1999-V-10 hot plate (ChemGlass Life Sciences, LLC, Vineland, NJ).

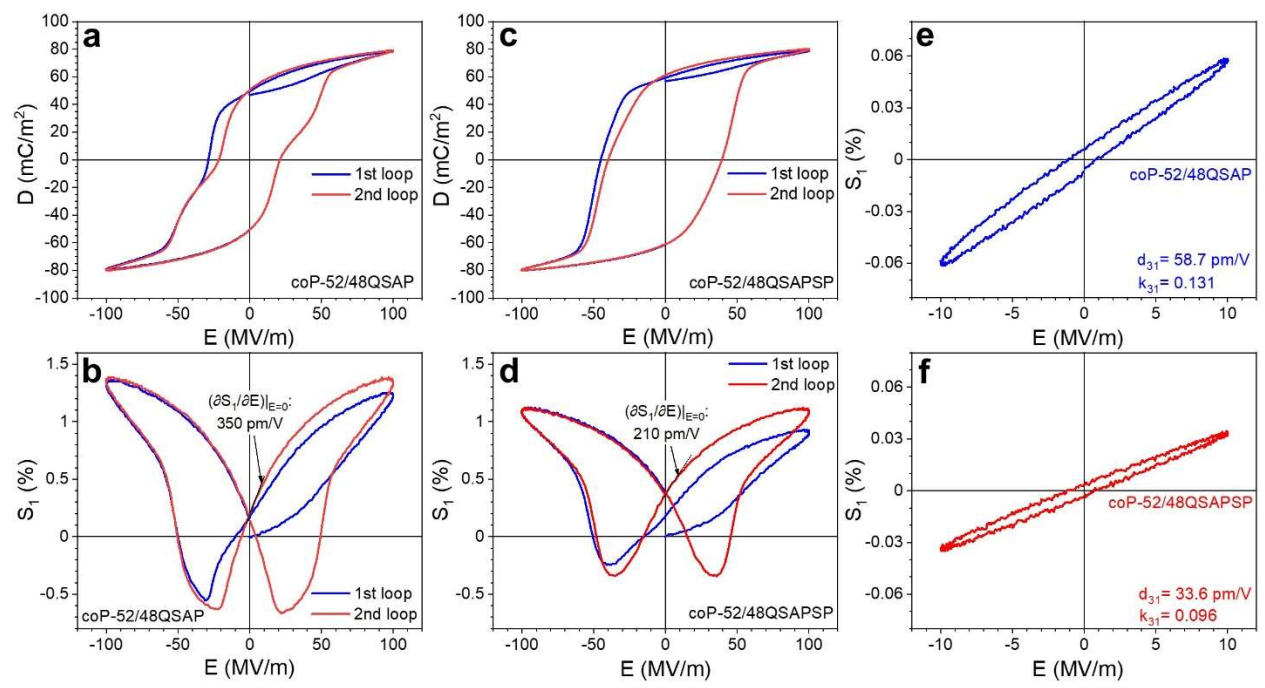


Figure 1. Two continuous bipolar (a,c) D-E and (b,d) S_1 -E loops for (a,b) coP-52/48 QSAP and (c,d) coP-52/48 QSAPSP films. The poling frequency was 1 Hz with a sinusoidal waveform. Determination of the inverse piezoelectric coefficient d_{31} and the electromechanical coupling factor k_{31} using bipolar S_1 -E loops at 10 MV/m for (e) coP-52/48 QSAP and (f) coP-52/48 QSAPSP films. All tests were performed at room temperature.

Result and Discussion

Different Piezoelectric Properties of the coP-52/48QSAP and coP-52/48QSAPSP

Films. Figures 1a-d show the first two continuous bipolar D-E and S₁-E loops at 100 MV/m for the coP-52/48QSAP and coP-52/48QSAPSP films. Although the maximum D values of these two samples were almost the same (around 80 mC/m²), the hysteresis loop of coP-52/48QSAPSP became more ferroelectric (i.e., with a higher coercive field, $E_C = 39$ MV/m) than the double hysteresis loop of coP-52/48QSAP ($E_C = 21$ MV/m). According to recently reports, $^{21, 24, 32}$ the in-situ slope at E=0 [($\partial S_1/\partial E$)| $_{E=0}$] in the returning S_1 -E loops during high-field (e.g., above the E_C at 100 MV/m) bipolar poling could be calculated (Figures 1b,d). In the returning loops, a large in-situ remanent polarization (P_r) persists at E=0. Because piezoelectricity is the electrostriction under a bias polarization, $^{9, 12, 13}$ this in-situ slope at E=0 could be considered as an indicator for the

piezoelectric effect. As we can see, the in-situ slope of coP-52/48QSAPSP (~210 pm/V) was significantly lower than that of coP-52/48QSAP (~350 pm/V). Meanwhile, the overall actuation strain (i.e., $\Delta S_1 = S_{1,max} - S_{1,min}$) during the second bipolar poling also decreased for coP-52/48QSAPSP ($\Delta S_1 = 1.45\%$), as compared with coP-52/48QSAP ($\Delta S_1 = 2.05\%$, see Figures 1b,d). Note that in-situ slope at E=0 could be used to show the upper limit of the piezoelectric performance, as discussed before.²⁴ In practical applications, ex-situ d₃₁ should be used. The ex-situ inverse d_{31} was determined by the slope of the linear S_1 -E loop at a low electric field (e.g., below the E_C at 10 MV/m, Figures 1e,f). Again, the ex-situ d₃₁ of coP-52/48QSAPSP (33.6 pm/V) was also lower than that of coP-52/48QSAP (58.7 pm/V). Based on the Young's modulus (Y₁) of coP-52/48QSAP at room temperature (1.1 GPa, see Figure S1 in the Supporting Information), the electromechanical coupling factor k₃₁ values were calculated to be 0.131 and 0.096 for coP-52/48QSAP and coP-52/48QSAPSP, respectively. From these results, it is interesting to see that additional stretching (6%) and electric poling (100 MV/m for 20 times) of the coP-52/48QSAP film resulted in drastically different ferroelectric property and piezoelectric performance.

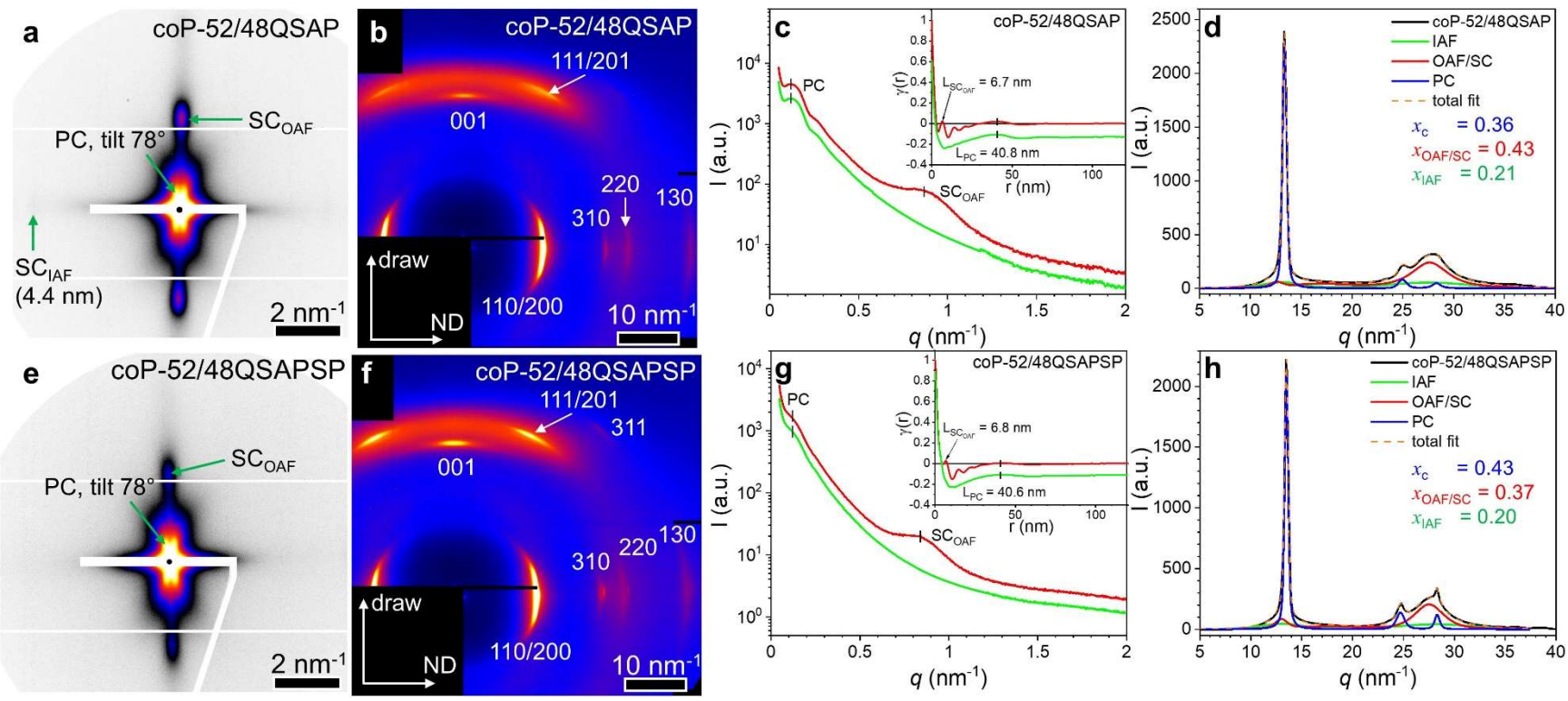
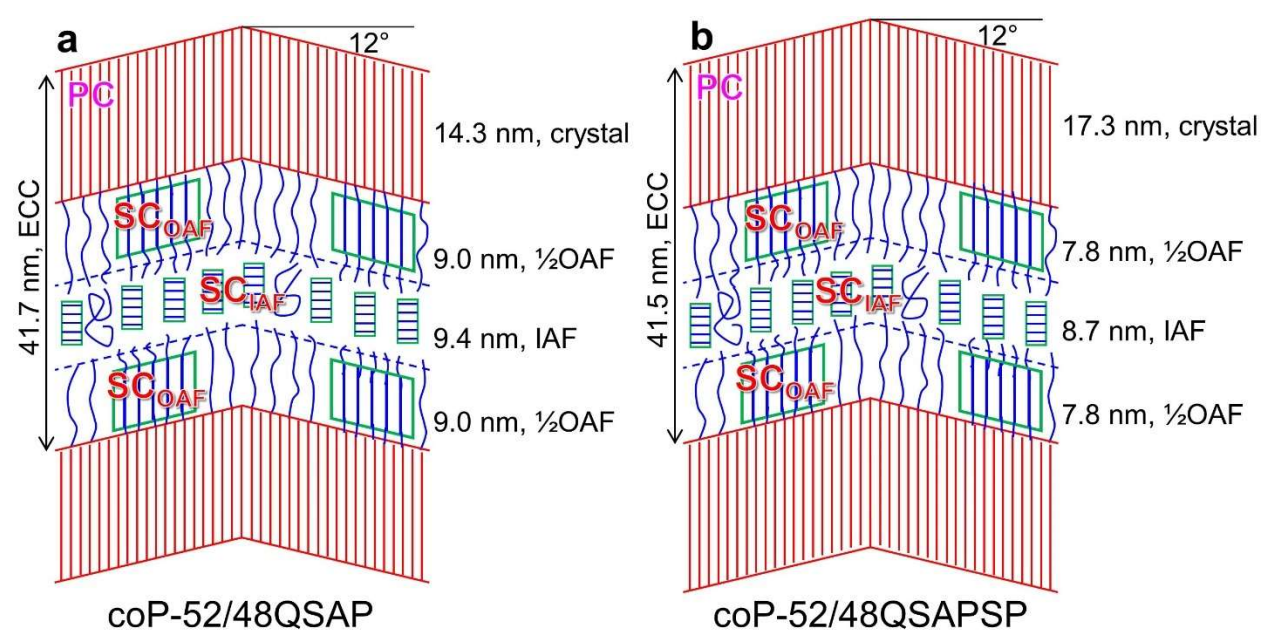


Figure 2. 2D edge-on (a,e) SAXS and (b,f) WAXD patterns for (a,b) coP-52/48QSAP and (e,f) coP-52/48QSAPSP, respectively. ND: normal direction of the film. 1D SAXS profiles and corresponding 1D correlation function curves (in the insets) for (c) coP-52/48QSAP and (g) coP-52/48QSAPSP (red curves). The green curves are 1D SAXS profile without the SC_{OAF} peak and the corresponding correlation function curve (in the insets). Both green SAXS and correlation function curves are offset from the corresponding red curves to avoid overlapping. Determination of x_c , x_{OAF} , and x_{IAF} for (d) coP-52/48QSAP and (h) coP-52/48QSAPSP from the WAXD results using the PeakFit software. The Gaussian + Lorentzian area function is used for the peak-fitting.

Semicrystalline Structures of coP-52/48QSAP and coP-52/48QSAPSP. To understand the underlying mechanism of drastically different ferroelectric and piezoelectric properties between coP-52/48QSAP and coP-52/48QSAPSP, structural characterization using synchrotron SAXS and WAXD was carried out. Figures 2a,e show 2D SAXS patterns for coP-52/48QSAP and coP-52/48QSAPSP, respectively. Both patterns exhibited close similarity. i) A butterfly pattern was observed for the primary crystal (PC) lamellae with a tilt angle of 78° from the stretching direction (see Scheme 1). ii) A tear drop-like scattering was observed on the meridian. From our recent report, ²⁴ it was ascribed to the form-factor scattering from SC_{OAF} (Scheme 1). In addition, a fairly weak scattering peak was also observed on the equator for coP-52/48QSAP with a spacing of 4.4 nm. It was ascribed to the scattering from SCs in the IAF layer (SC_{IAF}, see Scheme 1).²⁴ To obtain the overall PC lamellar spacing (L_{PC}), 1D correlation function analysis was performed based on the integrated 1D SAXS curves in Figures 2c,g for coP-52/48QSAP and coP-52/48QSAPSP. The correlation function results are presented in the insets. When both scattering peaks from PC and SC_{OAF} were present, the 1D correlation function curves (red) exhibited wiggles at the low distance (r). To understand this observation, the SC_{OAF} scattering peak was removed artificially; see the green SAXS curves in Figures 2c,g. Intriguingly, the wiggles disappeared and L_{PC} could be determined at the first maximum of the correlation function curves; see the offset green correlation function curves in the insets of Figures 2c,g: $L_{PC} = 40.8$ nm for coP-52/48QSAP and L_{PC} = 40.6 nm for coP-52/48QSAPSP. If this is the case, then the wiggles in the correlation function curves should originate from the SC_{OAF} scattering peak. The dimensions of the SC_{OAF} (L_{SC,OAF}) were determined from the first maximum in the red correlation function curves: $L_{SC,OAF} = 6.7$ nm for coP-52/48QSAP and $L_{SC,OAF} = 6.8$ nm for coP-52/48QSAPSP.

Figures 2b,d show 2D WAXD patterns for coP-52/48QSAP and coP-52/48QSAPSP,

respectively. Again, both patterns showed close similarity. i) Oriented PC reflections of the low-temperature ferroelectric phase (having an orthorhombic structure²⁷) were observed and assigned. The PC reflections for coP-52/48QSAPSP appeared to be stronger than those for coP-52/48QSAP. ii) Around the PC reflections, halo-like scatterings were observed, which could be attributed to the scatterings from both OAF and SCs (including both SC_{OAF} and SC_{IAF}). Note that the structures of SCs should also be fairly poor, and we could not differentiate the SC scattering from the OAF scattering in the WAXD of these samples. From the 2D WAXD analysis, ^{24, 31} the contents of PCs (x_c), OAF and SCs ($x_{OAF/SC}$), and IAF (x_{IAF}) could be determined. An example 2D WAXD analysis is given in Figure S2 for coP-52/48QSAPSP. Using peak-fitting, results for coP-52/48QSAP and coP-52/48QSAPSP are shown in Figures 2d,h, respectively. For coP-52/48QSAP, $x_c = 0.36$, $x_{OAF/SC} = 0.43$, and $x_{IAF} = 0.21$. For coP-52/48QSAPSP, $x_c = 0.43$, $x_{OAF/SC} = 0.37$, and $x_{IAF} = 0.20$. As we can see, the x_{IAF} values remained the same around 0.20 for both coP-52/48QSAPSP and coP-52/48QSAPSP. However, after additional stretching and electric poling, coP-52/48QSAPSP had a higher x_c and a lower $x_{OAF/SC}$.



Scheme 1. Schematic semicrystalline structures for (a) coP-52/48QSAP and (b) coP-52/48QSAPSP films. Note, polymer chains in the IAF layer are largely omitted to avoid crowdedness.

Based on our previous report,²⁴ the densities of PC, OAF, and IAF in coP-52/48QSAP are estimated to be 1.916, 1.843, and 1.770 g/cm³, respectively. Using these densities and combining the above SAXS and WAXD results, the three-phase semicrystalline structures of coP-52/48QSAP and coP-52/48QSAPSP are presented in Schemes 1a,b, respectively. Again, both structures bear close similarity. i) The PCs adopt an ECC structure. ii) SC_{OAF} is induced by electric poling (at 100 MV/m) in the OAF layers. iii) In the IAF layers, certain SC_{IAF} are present; however, the crystal orientation is 90° from that of both PCs and SC_{OAF}. Different from coP-52/48QSAP (Scheme 1a), the PC lamellae become thicker, and the OAF layers become thinner for coP-52/48QSAPSP (Scheme 1b). Obviously, after additional 6% mechanical drawing and 100 MV/m electric poling of coP-52/48QSAP, stretching-induced crystallization happened by crystallizing the OAF chains at the PC/OAF interfaces into the PCs. Then, we ask a question: could this morphological difference affect the ferroelectric and piezoelectric properties of coP-52/48QSAPSP? Further experimental studies need be performed to answer this question.

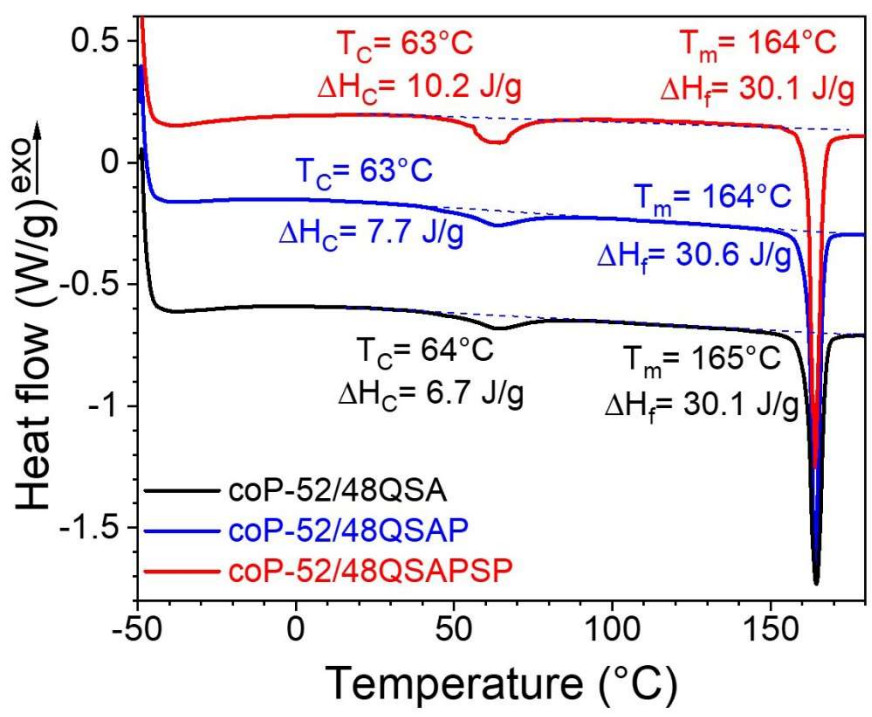


Figure 3. First heating DSC curves for coP-52/48QSA, coP-52/48QSAP, and coP-52/48QSAPSP. The heating rate was 10 °C/min.

Figure 3 shows the first heating DSC curves for coP-52/48QSA, coP-52/48QSAP, and coP-52/48QSAPSP films. The melting temperatures (T_m, around 164 °C) and heats of fusion (ΔH_f, around 30.3 J/g) for the paraelectric PCs in these samples were almost the same. However, the heats of transition around 63 °C, which included both the Curie transition and the SC melting, ²⁴ increased from 6.7 J/g for coP-52/48QSA to 7.7 J/g for coP-52/48QSAP, and to 10.2 J/g for coP-52/48QSAPSP. As reported before, ²⁴ there were hardly any SCs in coP-52/48QSA; therefore, the transition at 64 °C (6.7 J/g) was primarily attributed to the Curie transition of the ferroelectric PCs. For coP-52/48QSAP with the poling field-induced SC_{OAF}, the enhanced heat of transition (7.7 J/g) should be attributed to both the Curie transition of PCs and the melting of SCs. For coP-52/48QSAPSP with reduced OAF and SC_{OAF}, the further enhanced heat of transition (10.2 J/g) should be attributed to enhanced ferroelectricity with larger domains in PCs. Although this DSC

study confirmed the enhanced ferroelectricity of coP-52/48QSAPSP, it was still not clear whether the dipole mobility in SC_{OAF} was decreased or not.

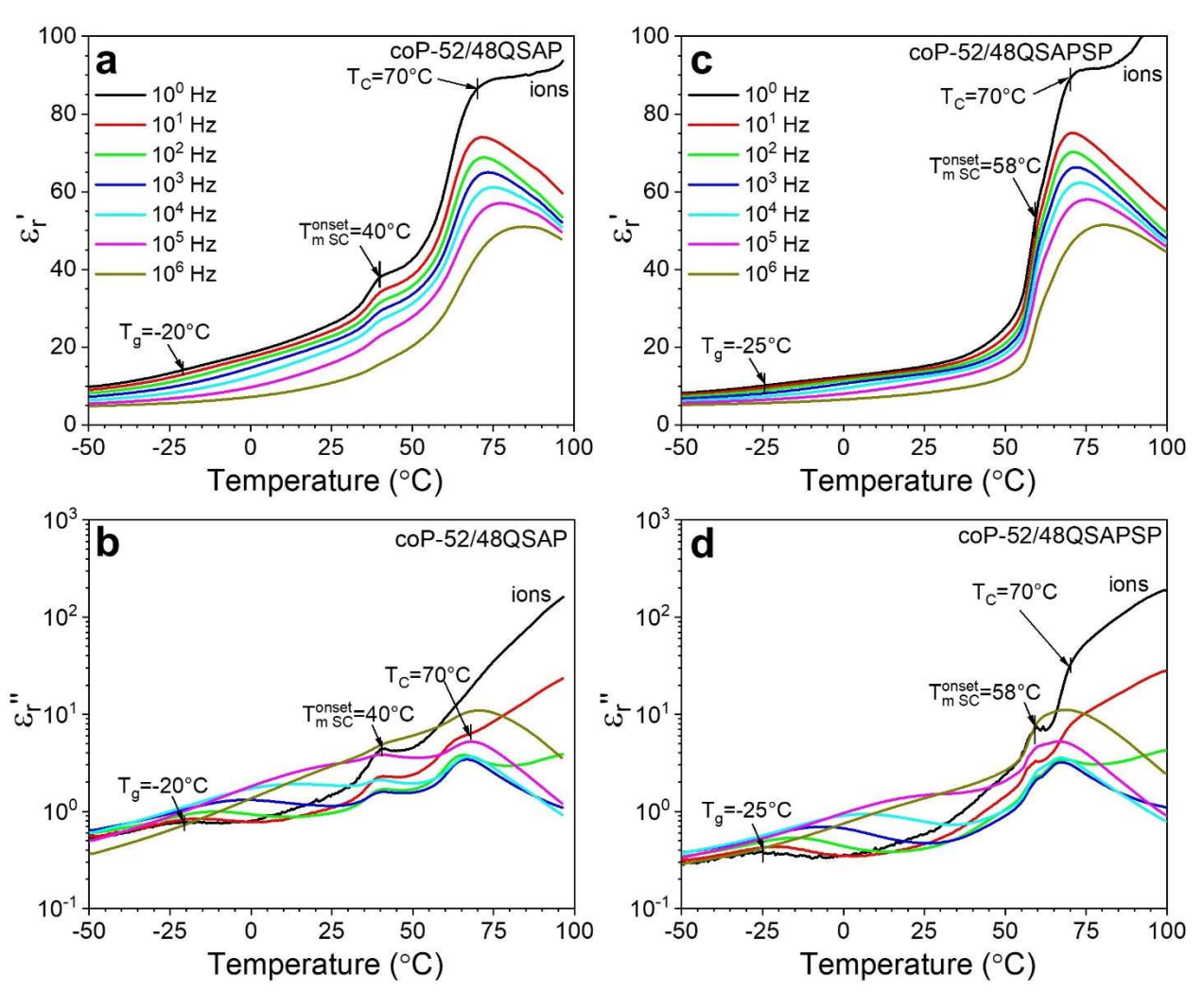


Figure 4. Temperature-scan BDS results of (a,c) ε_r ' and (b,d) ε_r " for (a,b) coP-52/48QSAP and (c,d) coP-52/48QSAPSP under different frequencies. The heating rate was 2 °C/min.

It is known that BDS is a powerful tool to study dipole mobility in polymers;³³ the higher the permittivity, the higher the dipole mobility, given the total number of dipoles keep constant. In this study, temperature-scan BDS study was carried out to directly investigate the dipole mobility for coP-52/48QSAP and coP-52/48QSAPSP (Figure 4). For coP-52/48QSAP, shoulder peaks in both ε_{r} and ε_{r} were seen around 40 °C at low frequencies (Figures 4a,b). Judging from

the DSC result in Figure 3, this temperature of 40 °C was the onset of SC_{OAF} melting. For coP-52/48QSAPSP, these shoulder peaks in ε_r' and ε_r'' shifted to a higher temperature of 58 °C (Figures 4c,d). From Figures 4a,c, at 25 °C the ε_r' values were 21.4 and 13.2 under 1 kHz for coP-52/48QSAP and coP-52/48QSAPSP, respectively. From Figure 2, the $x_{OAF/SC}$ of coP-52/48QSAPSP decreased 14% compared to that of coP-52/48QSAP. This could not account for the 42% decrease in the ε_r' value. Therefore, we could conclude that the dipole mobility in coP-52/48QSAPSP must be significantly reduced as compared to that in coP-52/48QSAP. Therefore, the lower piezoelectric performance of coP-52/48QSAPSP could be attributed to reduced dipole mobility in SC_{OAF} and decreased $x_{OAF/SC}$.

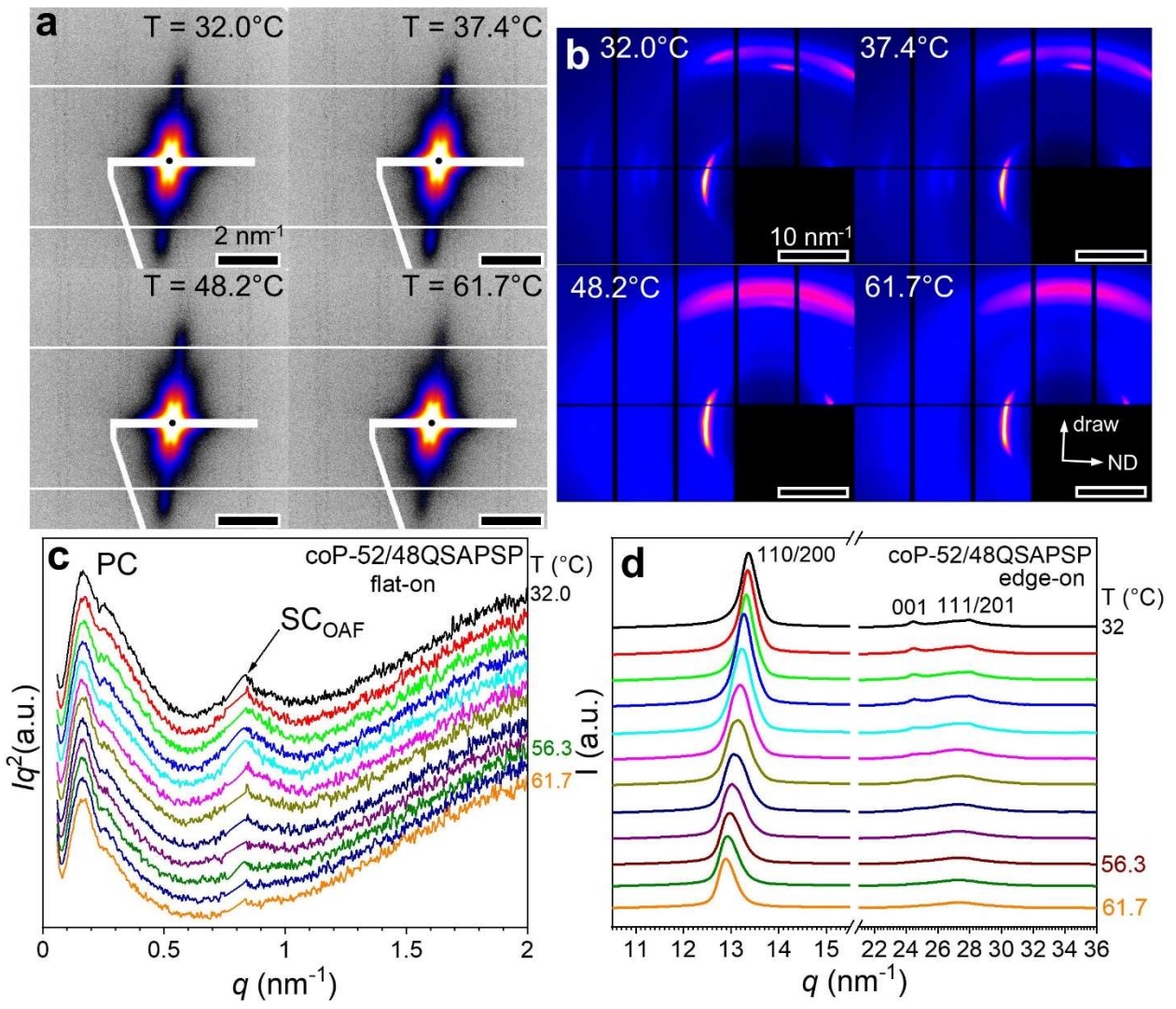


Figure 5. 2D in-situ (a) SAXS (flat-on) and (b) WAXD (edge-on) patterns for the coP-52/48QSAPSP film during heating at different temperatures. The heating rate was 2.5 °C/min. Integrated (c) 1D SAXS and (d) 1D WAXD curves for coP-52/48QSAPSP during heating at different temperatures. For (c) and (d), the temperature interval is about 2.7 °C.

The melting of SC_{OAF} around 60 °C for coP-52/48QSAPSP was directly confirmed by insitu 2D SAXS (flat-on) and WAXD (edge-on) during heating (Figures 5a,b). The integrated 1D SAXS and WAXD curves are shown in Figures 5c,d, respectively. When the temperature was lower than 50 °C, the intensity of the SC_{OAF} scattering peak slightly increased with increasing temperature. Above 50 °C, the intensity of the SC_{OAF} scattering peak decreased because of the melting of SC_{OAF}. With an increase in temperature, the position of the (110/200) reflection

gradually shifted to lower q values, indicating a gradual increase of its d-spacing when the temperature approached the Curie temperature. Meanwhile, the (001) and (111/201) reflections gradually weakened as well.

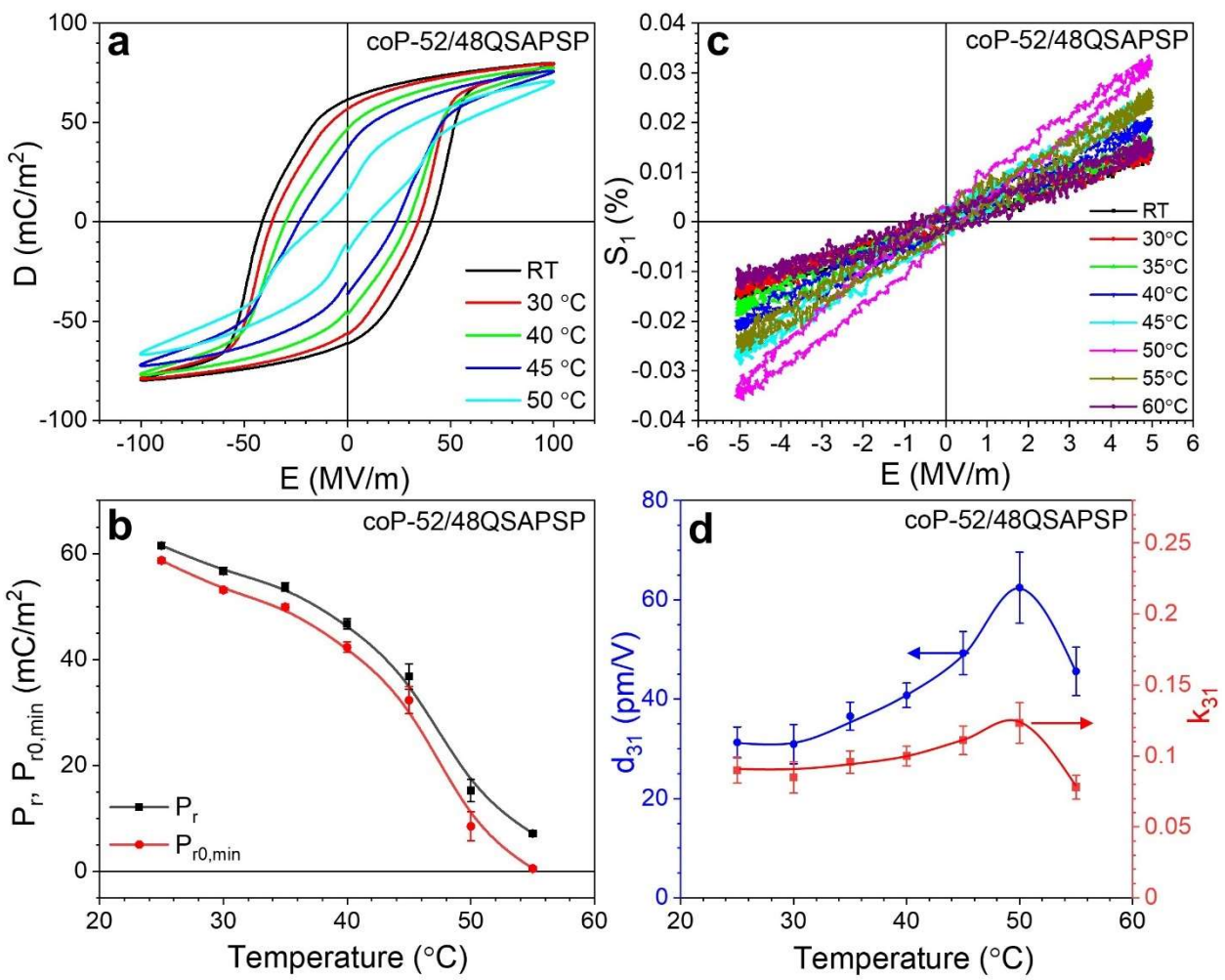


Figure 6. (a) Bipolar D-E loops at different temperatures. (b) Temperature dependent P_r and $P_{r0,min}$. P_r and $P_{r0,min}$ are determined from bipolar D-E loops in Figure S3. (c) Bipolar S_1 -E loops at different temperatures. The poling field was 5 MV/m at 1 Hz. (d) Temperature-dependent d_{31} and k_{31} . The d_{31} was obtained by the slope of the S_1 -E loops in (c).

Enhanced Piezoelectric Property of coP-52/48QSAPSP at Elevated Temperatures.

From the BDS result in Figure 4c, the ε_r' of coP-52/48QSAPSP increased significantly above 50 °C, indicating that the dipole mobility of SC_{OAF} could be regained upon increasing temperature.

Therefore, the effect of temperature on the piezoelectric performance of coP-52/48QSAPSP was Figure 6a shows the bipolar D-E loops of coP-52/48QSAPSP at different temperatures. The in-situ P_r values were obtained from the centered second bipolar loops in Figure 6a, and the minimum P_{r0} (P_{r0,min}) values were obtained from Figure S3. As shown in Figure 6b, the in-situ P_r and P_{r0,min} monotonously decreased with increasing temperature. Finally, when the temperature reached 55 °C, P_{r0,min} dropped to nearly zero. Bipolar S₁-E loops at different temperatures are shown in Figure 6c. The poling electric field was 5 MV/m at 1 Hz. The ex-situ d₃₁ values were obtained from Figure 6c and are presented in Figure 6d. When the temperature was lower than 35 °C, the ex-situ d₃₁ kept nearly unchanged (around 31.3 pm/V). When the temperature was higher than 35 °C, the ex-situ d₃₁ increased sharply as the temperature raised and reached a maximum value of 62.5±7.2 pm/V at 50 °C. Above 50 °C, the SC_{OAF} melted and P_{r0,min} continued to decrease, resulting in a significantly drop of piezoelectric performance. The coupling factor k_{31} was determined from the Y_1 (Figure S1) and dielectric constant (ε_r ' at 1 Hz in Figure 4c) by $k_{31} = d_{31}[Y/(\varepsilon_r \varepsilon_0)]^{0.5}$, and results are shown in Figure 6d. A maximum value of 0.123 was achieved at 50 °C. From this study, we concluded that a high piezoelectric performance could be achieved in coP-52/48QSAPSP at elevated temperatures after regaining the dipole mobility in SC_{OAF}. Given the even higher d₃₁ (62.5 pm/V) of coP-52/48QSAPSP at 50 °C than that of coP-52/48QSAP (d₃₁ = 58.7 pm/V) at room temperature, we consider that the dipole mobility in SC_{OAF} should be more important than the $x_{OAF/SC}$ for the piezoelectricity of P(VDF-TrFE) random copolymers.

If we did not heat coP-52/48QSAPSP above 50 °C to fully melt SCs, the ex-situ d₃₁ was reversible during heating and cooling cycles between 25 and 50 °C (see Figure S4). However, from the first heating and first cooling temperature-scan BDS results (between -50 and 50 °C) in

Figure S5, the $\varepsilon_{r'}$ during cooling was higher than that during heating, indicating enhanced dipole mobility in the SCs and increased $x_{OAF/SC}$ upon heating. Meanwhile, the P_{r0} decreased after the first heating (see Figure 6b). As a result, the overall piezoelectricity during first cooling and second heating was similar to that during the first heating.

Conclusions

In summary, by comparing coP-52/48QSAP and coP-52/48QSAPSP, the effect of dipole mobility of SC_{OAF} on piezoelectricity was investigated. Based on structural analysis using SAXS and WAXD, the x_c increased 0.07 and $x_{OAF/SC}$ decreased 0.06 in coP-52/48QSAPSP as compared to coP-52/48QSAP. From the BDS study, the ε_r ', which could be an indicator of dipole mobility, was 13.2 at 1 kHz for coP-52/48QSAPSP, much lower than that of 21.3 at 1 kHz for coP-52/48QSAP. The significantly lower ε_r ' thus indicated a reduced dipole mobility in SC_{OAF} of coP-52/48QSAPSP. As a result, its piezoelectric performance drastically decreased at room temperature. However, upon heating to the SC_{OAF} melting (~58 °C) before the Curie transition temperature (~65 °C), the dipole mobility in SC_{OAF} largely regained. As a result, higher piezoelectric performance (d₃₁ = 62.5±7.2 pm/V and k₃₁ = 0.123) was obtained at 50 °C for coP-52/48QSAPSP. Above 50 °C, the SC_{OAF} melted and P_{r0,min} decreased to zero, leading to a significantly drop of the piezoelectric performance. The knowledge obtained from this study will help us further understand the role of SC_{OAF} on piezoelectricity of ferroelectric polymers, which is important for the future design of high-performance piezoelectric polymers.

Determination of Young's modulus from stress-strain curves at different temperatures, estimation of x_c , x_{OAF} , and x_{IAF} using 2D WAXD quantitative analysis, determination of in-situ P_r and minimum P_{r0} ($P_{r0,min}$) for coP-52/48QSAPSP at different temperatures. and piezoelectric performance and BDS during heating and cooling cycles.

Acknowledgments

L.Z. acknowledges financial support from National Science Foundation, Division of Materials Research, Polymers Program (DMR-2103196). H.H. acknowledges partial support by the National Natural Science Foundation of China (51873075). This research used the 11-BM CMS beamline of National Synchrotron Light Source-II (NSLS-II), Brookhaven National Laboratory (BNL), a U.S. Department of Energy User Facility operated for the Office of Science by BNL under Contract DE-SC0012704. The authors thank Dr. Masafumi Fukuto at NSLS-II of BNL for helping SAXS and WAXD experiments.

Conflict of Interest

The authors declare no conflict of interest.

References

- 1. Heywang, W.; Lubitz, K.; Wersing, W. *Piezoelectricity: Evolution and Future of a Technology*; Springer: Berlin, 2008.
- Jean-Mistral, C.; Basrour, S.; Chaillout, J. J. Comparison of Electroactive Polymers for Energy Scavenging Applications. Smart Mater. Struct. 2010, 19, 085012.
- 3. Lee, J. H.; Yoon, H. J.; Kim, T. Y.; Gupta, M. K.; Lee, J. H.; Seung, W.; Ryu, H.; Kim, S. W.

- Micropatterned P(VDF-TrFE) Film-Based Piezoelectric Nanogenerators for Highly Sensitive Self-Powered Pressure Sensors. *Adv. Funct. Mater.* **2015**, *25*, 3203-3209.
- Dagdeviren, C.; Joe, P.; Tuzman, O. L.; Park, K. I.; Lee, K. J.; Shi, Y.; Huang, Y.; Rogers, J.
 A. Recent Progress in Flexible and Stretchable Piezoelectric Devices for Mechanical Energy
 Harvesting, Sensing and Actuation. *Extreme Mech. Lett.* 2016, 9, 269-281.
- 5. Chen, X.; Han, X.; Shen, Q. D. PVDF-Based Ferroelectric Polymers in Modern Flexible Electronics. *Adv. Electron. Mater.* **2017**, *3*, 1600460.
- Azimi, B.; Milazzo, M.; Lazzeri, A.; Berrettini, S.; Uddin, M. J.; Qin, Z.; Buehler, M. J.;
 Danti, S. Electrospinning Piezoelectric Fibers for Biocompatible Devices. *Adv. Healthcare Mater.* 2020, *9*, 1901287.
- Abolhasani, M. M.; Naebe, M.; Amiri, M. H.; Shirvanimoghaddam, K.; Anwar, S.; Michels,
 J. J.; Asadi, K. Hierarchically Structured Porous Piezoelectric Polymer Nanofibers for Energy Harvesting. Adv. Sci. 2020, 7, 2000517.
- 8. Kepler, R. G. Ferroelectric, Pyroelectric, and Piezoelectric Properties of Poly(vinylidene fluoride). In *Ferroelectric Polymers: Chemistry, Physics, and Applications*; Nalwa, H. S., Ed., Marcel Dekker, Inc.: New York, 1995, Chapter 3, pp. 183-232.
- 9. Zhang, Q. M.; Huang, C.; Xia, F.; Su, J. Electric EAP. In *Electroactive Polymer (EAP)*Actuators as Artificial Muscles: Reality, Potential, and Challenges, 2nd ed.; Bar-Cohen, Y.,

 Ed., SPIE Press: 2004, Chapter 4, pp. 89-139.
- Ramadan, K. S.; Sameoto, D.; Evoy, S. A Review of Piezoelectric Polymers as Functional Materials for Electromechanical Transducers. Smart Mater. Struct. 2014, 23, 033001.
- 11. Liu, Y.; Wang, Q. Ferroelectric Polymers Exhibiting Negative Longitudinal Piezoelectric Coefficient: Progress and Prospects. *Adv. Sci.* **2020**, *7*, 1902468.

- 12. Furukawa, T.; Seo, N. Electrostriction as the Origin of Piezoelectricity in Ferroelectric Polymers. *Jpn. J. Appl. Phys.* **1990**, *29*, 675-680.
- Li, F.; Jin, L.; Xu, Z.; Zhang, S. J. Electrostrictive Effect in Ferroelectrics: An Alternative Approach to Improve Piezoelectricity. *Appl. Phys. Rev.* 2014, 1, 011103.
- 14. Broadhurst, M. G.; Davis, G. T.; Mckinney, J. E.; Collins, R. E. Piezoelectricity and Pyroelectricity in Polyvinylidene Fluoride A Model. *J. Appl. Phys.* **1978**, *49*, 4992-4997.
- Wada, Y.; Hayakawa, R. A Model Theory of Piezo- and Pyroelectricity of Poly(Vinylidene Fluoride) Electret. Ferroelectrics 1981, 32, 115-118.
- Furukawa, T.; Wen, J. X.; Suzuki, K.; Takashina, Y.; Date, M. Piezoelectricity and Pyroelectricity in Vinylidene Fluoride Trifluoroethylene Copolymers. *J. Appl. Phys.* 1984, 56, 829-834.
- 17. Broadhurst, M. G.; Davis, G. T. Physical Basis for Piezoelectricity in PVDF. *Ferroelectrics* **1984**, *60*, 3-13.
- 18. Randall, C. A.; Kim, N.; Kucera, J. P.; Cao, W.; Shrout, T. R. Intrinsic and Extrinsic Size Effects in Fine-Grained Morphotropic-Phase-Boundary Lead Zirconate Titanate Ceramics. *J. Am. Ceram. Soc.* **1998**, *81*, 677-688.
- 19. Liu, Y.; Aziguli, H.; Zhang, B.; Xu, W. H.; Lu, W. C.; Bernholc, J.; Wang, Q. Ferroelectric Polymers Exhibiting Behaviour Reminiscent of a Morphotropic Phase Boundary. *Nature* **2018**, *562*, 96-100.
- 20. Tashiro, K.; Kobayashi, M.; Tadokoro, H.; Fukada, E. Calculation of Elastic and Piezoelectric Constants of Polymer Crystals by a Point Charge Model: Application to Poly(vinylidene fluoride) Form I. *Macromolecules* 1980, 13, 691-698.
- 21. Katsouras, I.; Asadi, K.; Li, M. Y.; van Driel, T. B.; Kjaer, K. S.; Zhao, D.; Lenz, T.; Gu, Y.;

- Blom, P. M.; Damjanovic, D.; Nielsen, M. M.; de Leeuw, D. M. The Negative Piezoelectric Effect of the Ferroelectric Polymer Poly(vinylidene fluoride). *Nat. Mater.* **2016**, *15*, 78-84.
- 22. Huang, Y.; Rui, G.; Li, Q.; Allahyarov, E.; Li, R.; Fukuto, M.; Zhong, G.-J.; Xu, J.-Z.; Li, Z.-M.; Taylor, P. L.; Zhu, L. Enhanced Piezoelectricity From Highly Polarizable Oriented Amorphous Fractions in Biaxially Oriented Poly(vinylidene fluoride) With Pure β Crystals. *Nat. Commun.* 2021, 12, 675.
- 23. Rui, G.; Huang, Y.; Chen, X.; Li, R.; Wang, D.; Miyoshi, T.; Zhu, L. Giant Spontaneous Polarization for Enhanced Ferroelectric Properties of Biaxially Oriented Poly(vinylidene fluoride) by Mobile Oriented Amorphous Fractions. *J. Mater. Chem. C* **2021**, *9*, 894-907.
- 24. Zhu, Z.; Rui, G.; Li, Q.; Allahyarov, E.; Li, R.; Soulestin, T.; Domingues Dos Santos, F.; He, H.; Taylor, P.; Zhu, L. Electrostriction-Enhanced Giant Piezoelectricity via Relaxor-Like Secondary Crystals in Extended-Chain Ferroelectric Polymers. *Matter* 2021, revision under review.
- 25. Neidhofer, M.; Beaume, F.; Ibos, L.; Bernes, A.; Lacabanne, C. Structural Evolution of PVDF During Storage or Annealing. *Polymer* **2004**, *45*, 1679-1688.
- 26. Yang, L.; Ho, J.; Allahyarov, E.; Mu, R.; Zhu, L. Semicrystalline Structure Dielectric Property Relationship and Electrical Conduction in a Biaxially Oriented Poly(vinylidene fluoride) Film under High Electric Fields and High Temperatures. ACS Appl. Mater. Interfaces 2015, 7, 19894-19905.
- 27. Tashiro, K., Crystal Structure and Phase Transition of PVDF and Related Copolymers. In Ferroelectric Polymers: Chemistry, Physics, and Applications; Nalwa, H. S., Ed., Marcel Dekker: New York, 1995, Chapter 2, pp. 63-182.
- 28. Womes, M.; Bihler, E.; Einsenmenger, W. Dynamics of Polarization Growth and Reversal in

- PVDF Films. IEEE Trans. Dielectr. Electr. Insul. 1989, 24, 461-468.
- Cheng, Z. Y.; Xu, T. B.; Bharti, V.; Wang, S. X.; Zhang, Q. M. Transverse Strain Responses in the Electrostrictive Poly(vinylidene fluoride-trifluorethylene) Copolymer. *Appl. Phys. Lett.* 1999, 74, 1901-1903.
- 30. Wongwirat, T.; Wang, M.; Huang, Y.; Treufeld, I.; Li, R.; Laoratanakul, P.; Manuspiya, H.; Zhu, L. Mesophase Structure-Enabled Electrostrictive Property in Nylon-12-Based Poly(ether-block-amide) Copolymers. *Macromol. Mater. Eng.* **2019**, *304*, 1900330.
- 31. Wongwirat, T.; Zhu, Z.; Rui, G.; Li, R.; Laoratanakul, P.; He, H.; Manuspiya, H.; Zhu, L. Origins of Electrostriction in Poly(vinylidene fluoride)-Based Ferroelectric Polymers.

 *Macromolecules** 2020, 53, 10942-10954.
- 32. Hafner, J.; Benaglia, S.; Richheimer, F.; Teuschel, M.; Maier, F. J.; Werner, A.; Wood, S.; Platz, D.; Schneider, M.; Hradil, K.; Castro, F. A.; Garcia, R.; Schmid, U. Multi-scale Characterisation of a Ferroelectric Polymer Reveals the Emergence of a Morphological Phase Transition Driven by Temperature. *Nat. Commun.* 2021, 12, 152.
- 33. Kremer, F.; Schönhals, A. Broadband Dielectric Spectroscopy; Springer: Berlin, 2003.